

# THE CHORUS NEUTRINO OSCILLATION EXPERIMENT

Dirk Rondeshagen  
Institut für Kernphysik  
University of Münster  
Wilhelm-Klemm-Strasse 9  
D-48149 Münster  
Germany  
rondesh@uni-muenster.de

Representing the CHORUS Collaboration

## ABSTRACT

The CHORUS (**C**ERN **H**ybrid **O**scillation **R**esearch apparatus) experiment is a short baseline neutrino oscillation experiment. It is performed in the CERN SPS wide-band neutrino beam and is sensitive to the transition  $\nu_\mu \rightarrow \nu_\tau$ . CHORUS is a hybrid detector which consists of an emulsion target followed by a real-time electronic detector. Data taking started in April 1994 and was completed in November 1997. With the full data sample of four years, CHORUS will reach a sensitivity in the  $\nu_\mu/\nu_\tau$  mixing angle down to  $\sin^2(2\theta_{\mu\tau}) \leq 2 \cdot 10^{-4}$  for large  $\Delta m^2$ . In the presently ongoing analysis, about 16,000 events found in the emulsion have been analyzed, resulting in a preliminary upper limit  $\sin^2(2\theta_{\mu\tau}) \leq 4.5 \times 10^{-3}$ .

# 1 Introduction

Even more than 60 years after the neutrino was first introduced, it is not known whether neutrinos have mass, despite its profound implication for particle physics, astrophysics, and cosmology.<sup>1</sup> A massive neutrino could well be a Dark Matter candidate<sup>2</sup> in the universe. Since neutrinos were produced in great numbers during the early phases after the Big Bang, even a small mass in the region of some tens of eV could provide closure of the universe. Oscillation experiments are the most promising way to obtain information about neutrino masses. The concept of neutrino oscillation was originally introduced by Pontecorvo<sup>3</sup> postulating the process  $\nu \rightarrow \bar{\nu}$ . After the discovery of  $\nu_\mu$ , the concept was extended for transitions between different neutrino flavors.<sup>4</sup>

The relation between the weak eigenstates ( $\nu_e, \nu_\mu, \nu_\tau$ ) and the mass eigenstates ( $\nu_1, \nu_2, \nu_3$ ) is given by a unitary matrix  $\mathbf{U}$ :

$$\begin{pmatrix} \nu_e \\ \nu_\mu \\ \nu_\tau \end{pmatrix} = \mathbf{U} \cdot \begin{pmatrix} \nu_1 \\ \nu_2 \\ \nu_3 \end{pmatrix}.$$

In the case of two-flavor mixing, here  $\nu_\mu$  and  $\nu_\tau$ , the relation between the different eigenstates is

$$\begin{pmatrix} \nu_\mu \\ \nu_\tau \end{pmatrix} = \begin{pmatrix} \cos \theta_{\mu\tau} & \sin \theta_{\mu\tau} \\ -\sin \theta_{\mu\tau} & \cos \theta_{\mu\tau} \end{pmatrix} \cdot \begin{pmatrix} \nu_1 \\ \nu_2 \end{pmatrix},$$

and the oscillation probability is given by

$$P(\nu_\mu \rightarrow \nu_\tau) = \sin^2(2\theta_{\mu\tau}) \cdot \sin^2\left(\frac{1.27 \cdot |m_\mu^2 - m_\tau^2| [eV^2] \cdot L [km]}{E [GeV]}\right),$$

where  $\theta_{\mu\tau}$  is the mixing angle,  $E$  the neutrino energy, and  $L$  the distance between the source and the detector.

## 2 Principle of Detection

The CHORUS experiment<sup>5</sup> searches for a charged current (CC) interaction of a  $\nu_\tau$  from a  $\nu_\mu \rightarrow \nu_\tau$  oscillation producing a negative  $\tau$ -lepton,

$$\nu_\tau + N \rightarrow \tau^- + X,$$

whereby it will be sensitive to the following decay channels of the  $\tau^-$ :

$$\begin{aligned} \tau^- &\rightarrow \mu^- \bar{\nu}_\mu \nu_\tau && (17.3\%) \\ &\rightarrow h^-(n\pi^0)\nu_\tau && (49.8\%) \\ &\rightarrow (\pi^+\pi^-\pi^-)(n\pi^0)\nu_\tau && (14.9\%). \end{aligned}$$

CHORUS is a classical appearance experiment. It uses the fact that the contamination of the CERN neutrino beam with tau neutrinos is negligible.

Because of the short lifetime of the tau ( $c\tau \sim 90 \mu\text{m}$ ), its unambiguous identification is, however, nontrivial. An elaborate hybrid technique is used to directly identify the tau track and its decay topology inside photographic emulsion.

The neutrinos from the tau decay will give rise to a “kink” topology between the  $\tau^-$  and its daughter for the muonic and singly charged hadron channel. The decay into three charged pions shows a three-prong topology, where the undetected neutrino will create an imbalance in the measured transverse momentum.

## 3 The CHORUS Experiment

### 3.1 The CERN Wide-Band Neutrino Beam

Neutrinos are produced in the CERN West Area Neutrino Facility<sup>7</sup> with a mean energy of about 27 GeV.

Protons in the SPS are accelerated to 450 GeV during a cycle of 14.4 s. They are extracted in two spills of 6 ms length separated by 2.5 s and directed onto a beryllium target. The delivered intensity is typically  $\sim 2.2 \times 10^{13}$  protons on target per SPS cycle.

The beryllium target consists of 11 beryllium rods positioned longitudinally along the beam direction and separated by 9 cm gaps. Each rod is 10 cm long and 3 mm in diameter. The geometry of the beryllium target corresponds to  $\sim 2.7$  interaction lengths.

Secondary positive pions and kaons are focused by a pair of magnetic lenses (the horn and reflector) into the 290 m decay tunnel, whereas negatively charged particles are defocused and escape from the beamline. In the decay tunnel, the particles decay mainly into  $\mu^+$  and  $\nu_\mu$ . The following shielding ( $\sim 370$  m) of iron

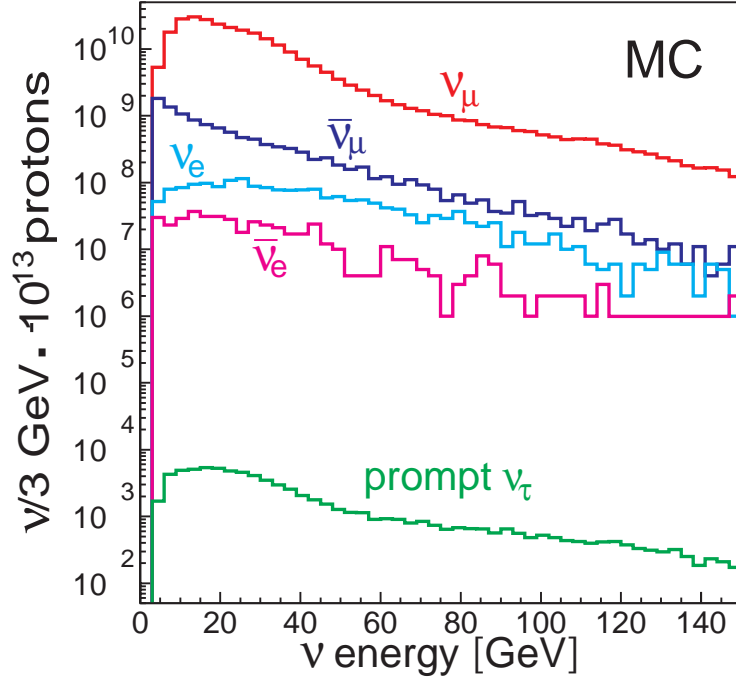


Figure 1: Neutrino energy distribution of the CERN Wide-Band Neutrino Beam in the CHORUS emulsion target [transverse dimension  $(1.44 \times 1.44) \text{ m}^2$ ].

and earth stops muons and other charged particles. The mean distance between the  $\nu$ -source and detector is 600 m.

The  $\nu_e$ 's and  $\bar{\nu}_e$ 's are produced in the electronic K decay and the  $\bar{\nu}_\mu$ 's originate from the decay of negative pions and kaons that are still in the beam. The contamination of the beam with  $\bar{\nu}_\mu$ ,  $\nu_e$ , and  $\bar{\nu}_e$  is less than 5%. The  $\nu_\tau$  contamination<sup>8</sup> in the beam from the prompt reaction

$$p + N \rightarrow D_s^- + X; \quad D_s^- \rightarrow \tau^- + \bar{\nu}_\tau,$$

followed by  $\tau^- \rightarrow \nu_\tau + X$ , is shown in Fig. 1. It is about six orders of magnitude lower than the  $\nu_\mu$  rate. The expected number of  $\nu_\tau$  interactions in the emulsion coming from the  $\nu_\tau$  beam contamination is 0.1 in four years and therefore negligible.

### 3.2 The CHORUS Detector

To identify the short flight path of the  $\tau^-$  lepton and its decay topology, CHORUS uses  $\sim 800 \text{ kg}$  of nuclear emulsion as an active target. Nuclear emulsion offers

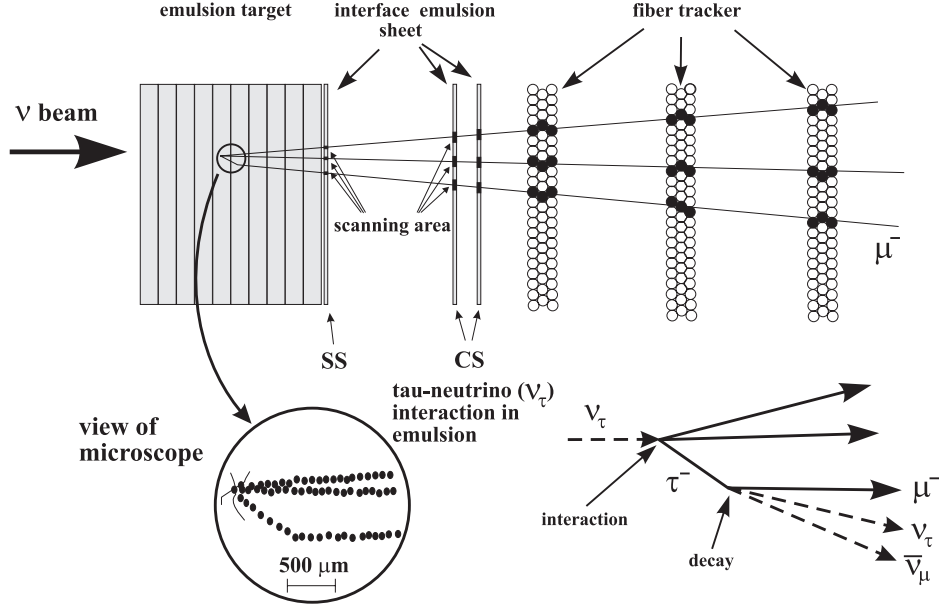


Figure 2: The target region with an emulsion target, three interface emulsion sheets (CS and SS), and three fiber trackers is shown schematically. A  $\nu_\tau$ -CC interaction with a “kink” structure which would be visible under the microscope is shown.

a spatial resolution of  $\sim 1 \mu\text{m}$  with a hit density of  $\sim 300/\text{mm}$  and is therefore ideal for detection of short-lived particles. The emulsion target is divided into four stacks with an area of  $(1.44 \times 1.44) \text{ m}^2$  and a thickness of 2.75 cm. Each stack is subdivided into eight modules with 35 plates with a thickness of  $800 \mu\text{m}$  each. Behind each module, there are three interface emulsion sheets. The first, the special sheet (SS), is directly mounted behind the emulsion target and the two others, the changeable sheets (CS), close to the target tracker. These interface sheets offer an angular resolution of  $\sim 1 \text{ mrad}$ . The scheme is depicted in Fig. 2.

The electronic part of the CHORUS detector combines several new techniques for track reconstruction, calorimetry, and particle identification. In the CHORUS target region, large arrays of scintillating fiber trackers are placed between the four emulsion stacks. Measured tracks in the scintillating fiber trackers are used to project the tracks onto the interface emulsion sheets, which act as an interface between the scintillating fiber trackers and the emulsion target. Through such an arrangement, track prediction accuracy progressively improves from the fiber

tracker to the CS and further down to the SS level right in front of the emulsion target.

Each of the eight scintillating fiber trackers<sup>9,10</sup> provides a position measurement in four projections. The fiber trackers offer a spatial accuracy of  $\sim 150 \mu\text{m}$  at the CS level and an angular accuracy of  $\sim 2 \text{ mrad}$ , in addition to a two-track resolution of about 1 mm.

The target region is followed by a magnetic spectrometer<sup>9,10</sup> (Fig. 3). It consists of an air-core magnet and three scintillating fiber trackers, one in front of and two behind the magnet. Here, the charge and momentum of low-energy particles are measured. The magnet operates in pulsed mode, synchronous to the two-spill beam extraction of the SPS. The magnetic spectrometer provides a momentum resolution of  $\Delta p/p \approx 0.3$  at 5 GeV.

The scintillating fibers of the target tracker and the magnetic spectrometer are  $500 \mu\text{m}$  in diameter and arranged in ribbons of seven layers. In total, about 1.1 million fibers with a total length  $\sim 2,500 \text{ km}$  are used. The readout is performed by 58 opto-electronic chains, each consisting of four image intensifiers and a CCD camera.

The emulsion target, the target trackers, and the magnetic spectrometer are placed inside a temperature-controlled cool box, which is kept at  $5^\circ\text{C}$  to reduce fading of the emulsion and aging of the scintillating fibers.

Further downstream, an  $e/\pi$  compensating calorimeter<sup>11</sup> follows the target region. A novel technique has been employed for the electromagnetic and the first half of the hadronic part of the calorimeter. Scintillating fibers of 1 mm diameter embedded in lead allow a fine-grain energy sampling and precise measurement of the energy flow vector. The second half of the hadronic calorimeter was built in layers of lead and scintillator planes. The energy resolution for electrons is  $\Delta E/E = 13\%/\sqrt{E}(\text{GeV})$  and for hadrons  $\Delta E/E = 32\%/\sqrt{E}(\text{GeV})$ .

A muon spectrometer is located behind the calorimeter. It consists of six magnetized iron toroid modules, each producing a magnetic field of  $\sim 1.8 \text{ T}$ . Tracking sections consisting of drift chambers and streamer tubes are sandwiched between the iron modules. The momentum resolution is about 10–20% for  $p < 100 \text{ GeV}$ . A sketch of the complete detector is shown in Fig. 3.

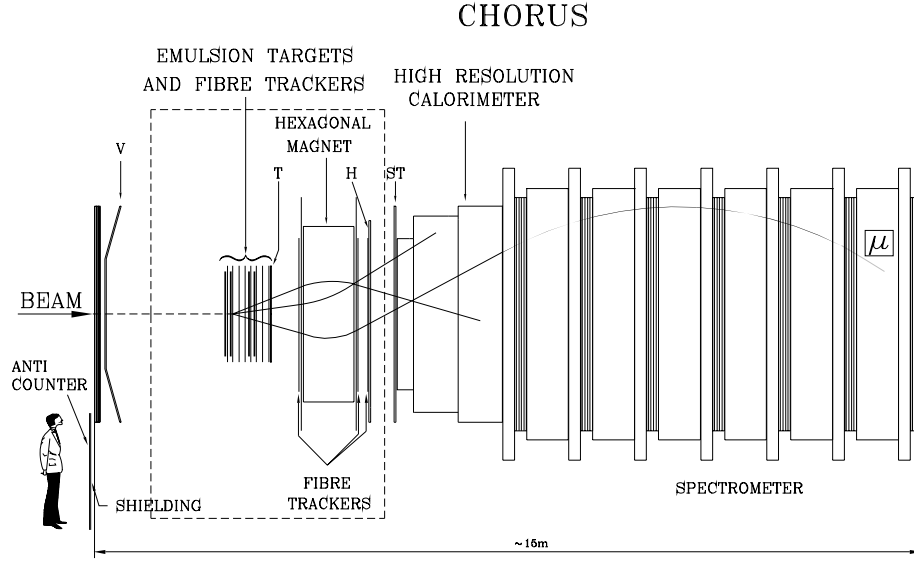


Figure 3: The CHORUS detector.

## 4 Analysis

### 4.1 Muon Decay Mode

In a first step, the muonic decay of the  $\tau^-$  is being searched for:

$$\begin{aligned} \nu_\tau + N &\rightarrow \tau^- + X \\ &\hookrightarrow \mu^- + \bar{\nu}_\mu + \nu_\tau. \end{aligned}$$

This decay channel offers a clear signature, since the muon can easily be recognized in the detector.

Only events with a reconstructed negative muon ( $p_{\mu^-} < 30$  GeV) and no other charged lepton are scanned in the emulsion.

To locate the event in the emulsion, the  $\mu^-$  track is searched for in the interface sheets. If found, the track is followed back into the emulsion target. On each upstream side of the emulsion plates, one tries to locate the entry point of the

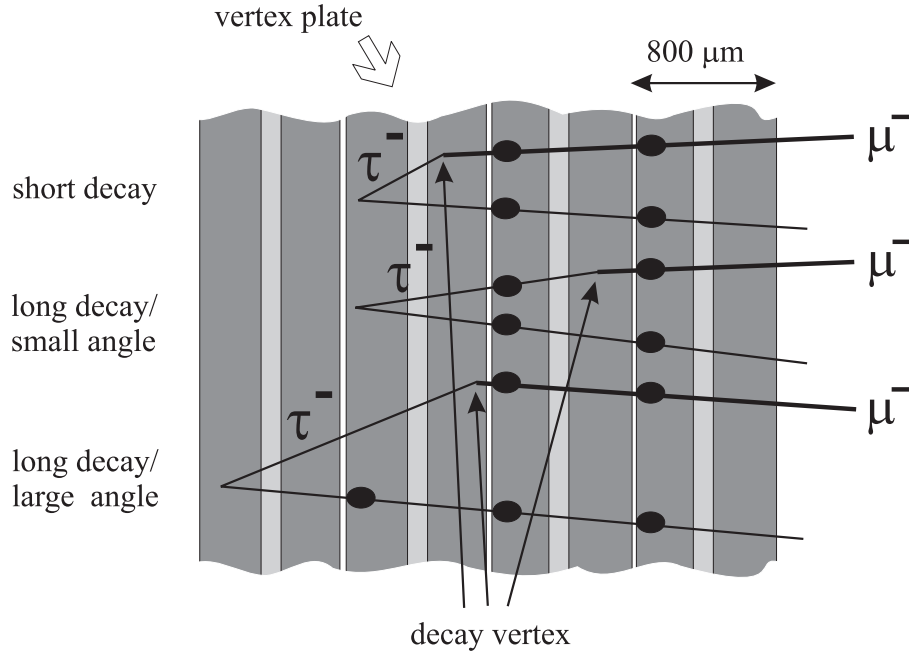


Figure 4: Classification of  $\tau$  decays into “short decay,” “long decay/small angle,” and “long decay/large angle” is shown schematically.

track. This is the scan back (SB) procedure. The first plate where the track cannot be verified anymore is called the “vertex plate,” assuming that a  $\nu$  interaction or a decay vertex is found in this plate.

If the  $\mu^-$  is the decay daughter of a  $\tau^-$ , three cases are possible (Fig. 4):

- A “short decay,” where the interaction vertex and decay vertex are in the same plate.
- A “long decay/small angle,” where the interaction vertex and decay vertex are in different plates, with a small angle between the parent and the daughter tracks (i.e., the “kink angle” is smaller than the tolerance of the “scan back” procedure of about 30–40 mrad).
- A “long decay/large angle,” where the interaction vertex and decay vertex are in different plates, with a large “kink angle” between the parent and the daughter tracks.

An overview of the scanning flow is illustrated in Fig. 5. If at least one further track belonging to the event is followed up to the “vertex plate,” a minimum

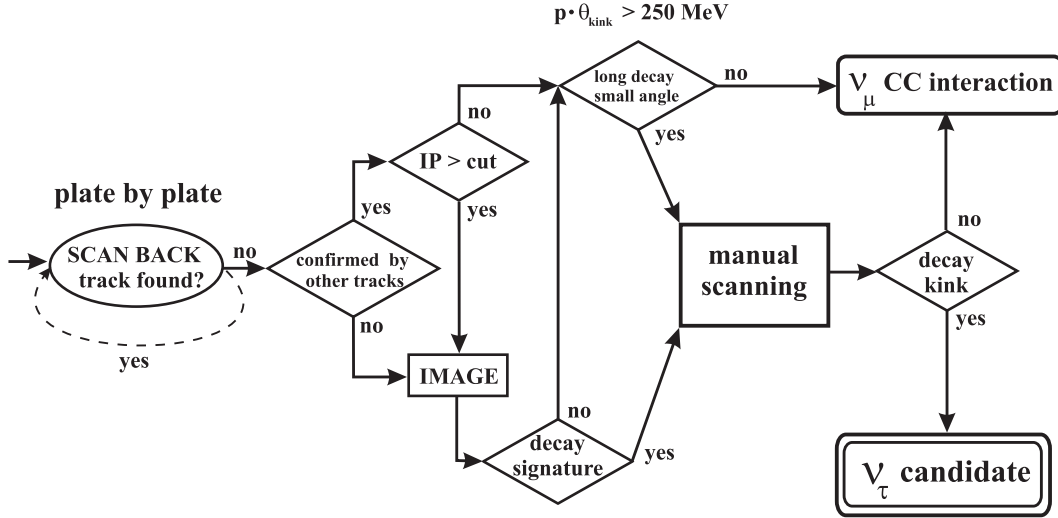


Figure 5: Scanning diagram.

distance (impact parameter) to the muon track can be determined to test the “short decay” hypothesis. In the case of a  $\nu_\mu$  interaction, all tracks are connected to the same vertex and this results in a zero impact parameter (Fig. 6). In a  $\nu_\tau$  interaction, the muon is produced at the secondary vertex, which results in a large impact parameter. For the “short decay” class, a selection on the impact parameter of bigger than 2–8  $\mu\text{m}$ , depending on the longitudinal position inside the plane, is applied.

A Monte Carlo simulation shows that 27% of all  $\tau$  decays are of the “short decay” type and 59% of these survive the selection cut (Fig. 7). If a large impact parameter is confirmed, a digital image is taken and the event is sent to offline analysis (video image analysis). It uses three-dimensional information from the full depth of the vertex plate.

For events with a small impact parameter, it has to be checked whether it belongs to the class “long decay/small angle.” Events with “kink angles” smaller than the scan-back tolerance can be confirmed by measuring the angular difference between the track at the vertex plate and the track in the special emulsion sheet (SS). If the measured transverse momentum  $p_t = p_\mu \cdot \theta_{kink}$  is larger than 250 MeV (Fig. 8), the event is scanned manually with computer assistance. For the “long decay/small angle” class, Monte Carlo data show that 88% of the tau events survive a cut on  $p_\mu \cdot \theta_{kink}$  (Fig. 9).

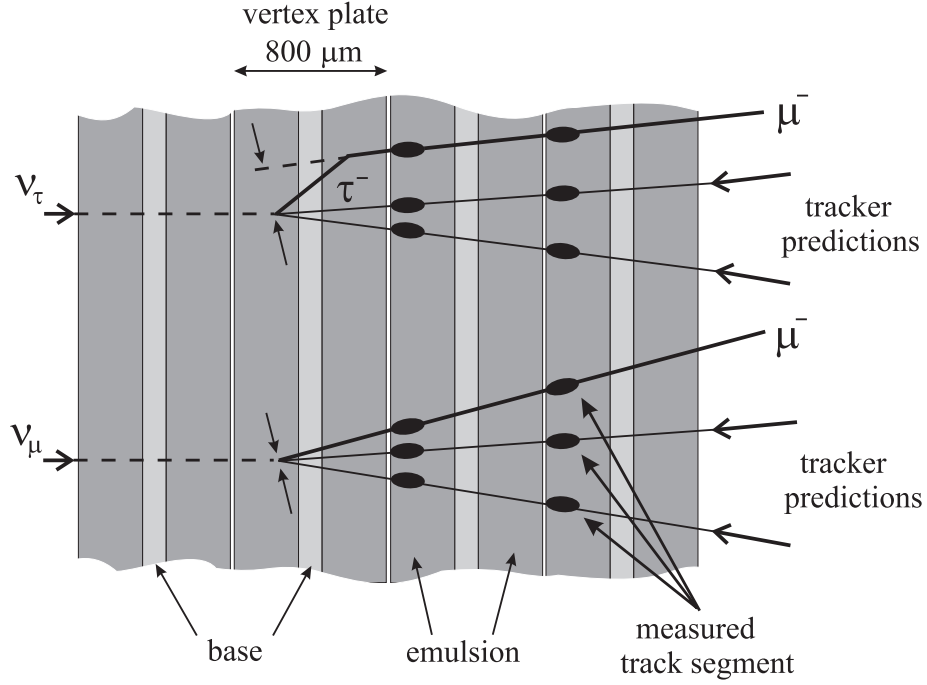


Figure 6: Comparison of the minimum distance (impact parameter) between  $\nu_\mu$ - and  $\nu_\tau$ -induced events for the “short decay” class.

For events where only one track was found or where the vertex plate was not confirmed by other tracks, an image of the vertex plate is taken. If no decay signature is found in the image analysis, the possibility of a “long decay/small angle” event is checked. If the “long decay/small angle” signature is not confirmed, this event is classified as a  $\nu_\mu$  interaction.

Decay angles larger than the scan-back tolerance (“long decay/large angle”), which are confirmed in the offline image analysis, are further investigated by eye scan.

The final kink analysis of events with a decay signature is done by eye scanning.

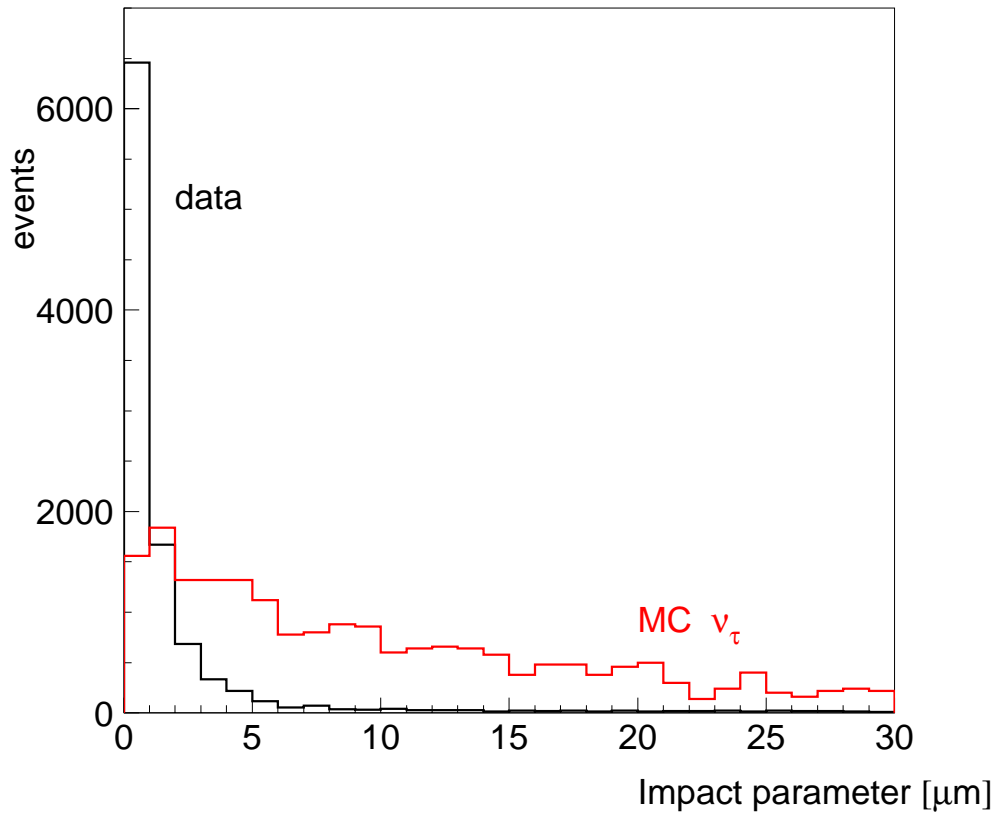


Figure 7: Distribution of the impact parameter from simulated  $\nu_\tau$  interactions and data. With a cut on the impact parameter of 2–8  $\mu\text{m}$ , 59% of the  $\nu_\tau$  interactions survive. A large fraction of data, mostly  $\nu_\mu$ -induced interactions, is cut.

## 4.2 Single Hadron Channel

A second analysis of the  $\tau^-$  decaying into a singly-charged negative hadron is under way:

$$\begin{aligned} \nu_\tau + N &\rightarrow \tau^- + X \\ &\hookrightarrow h^-(n\pi^0) + \nu_\tau. \end{aligned}$$

The scanning procedure and selection have evolved from those used for the  $\mu^-$  channel and are not described in detail here.

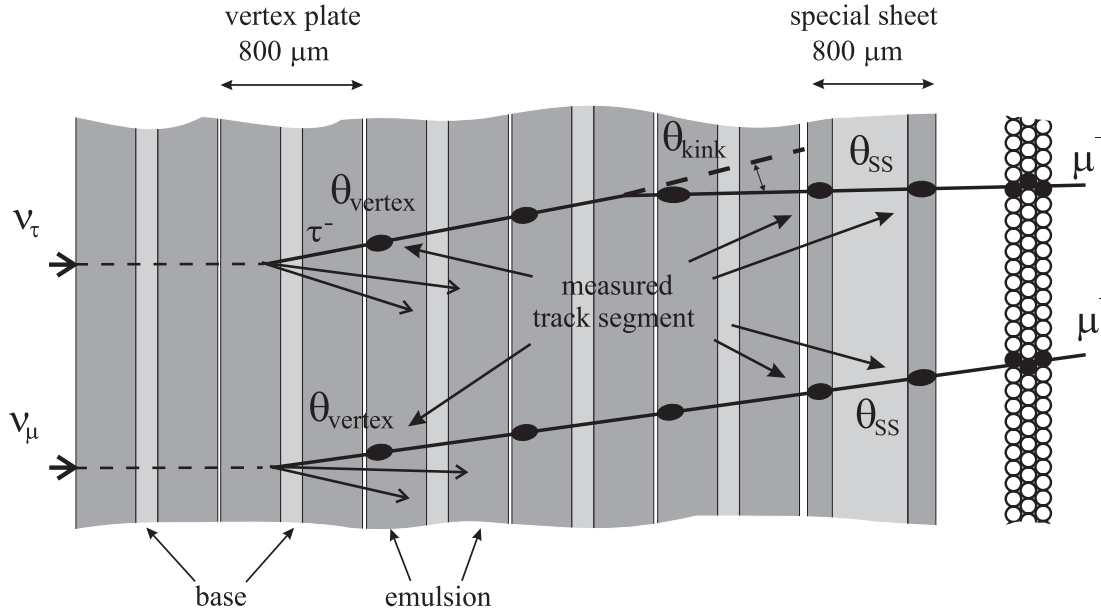


Figure 8: Comparison of the “kink angle” determination between  $\nu_{\mu^-}$  and  $\nu_{\tau^-}$  induced events for the “long decay/small angle” class.

Only events with a reconstructed negative hadron (momentum between 1 and 20 GeV) and no charged lepton will be scanned in the emulsion.

### 4.3 Background

As we are searching for a few, at most 60,  $\nu_{\tau^-}$ -induced events among  $10^6$   $\nu_{\mu^-}$  interactions, background sources have to be explored at a level down to  $10^{-7}$ .

- The main background for  $\tau^- \rightarrow \mu^-$  comes from:
  - muonic one-prong decay of charmed particles.
- The main backgrounds for  $\tau^- \rightarrow \text{hadron}^-(n\pi^0)$  come from:
  - hadron scattering without visible recoil (“white kink”)
  - one-prong decay of charmed particles.

One-prong muonic decays of negatively-charged charmed particles produced in  $\bar{\nu}_e$  or  $\bar{\nu}_{\mu}$  interactions contribute to the background if the primary lepton ( $e^+$  or  $\mu^+$ ) is not identified. This rate was estimated to be  $< 10^{-6} \times N^{CC}$ .

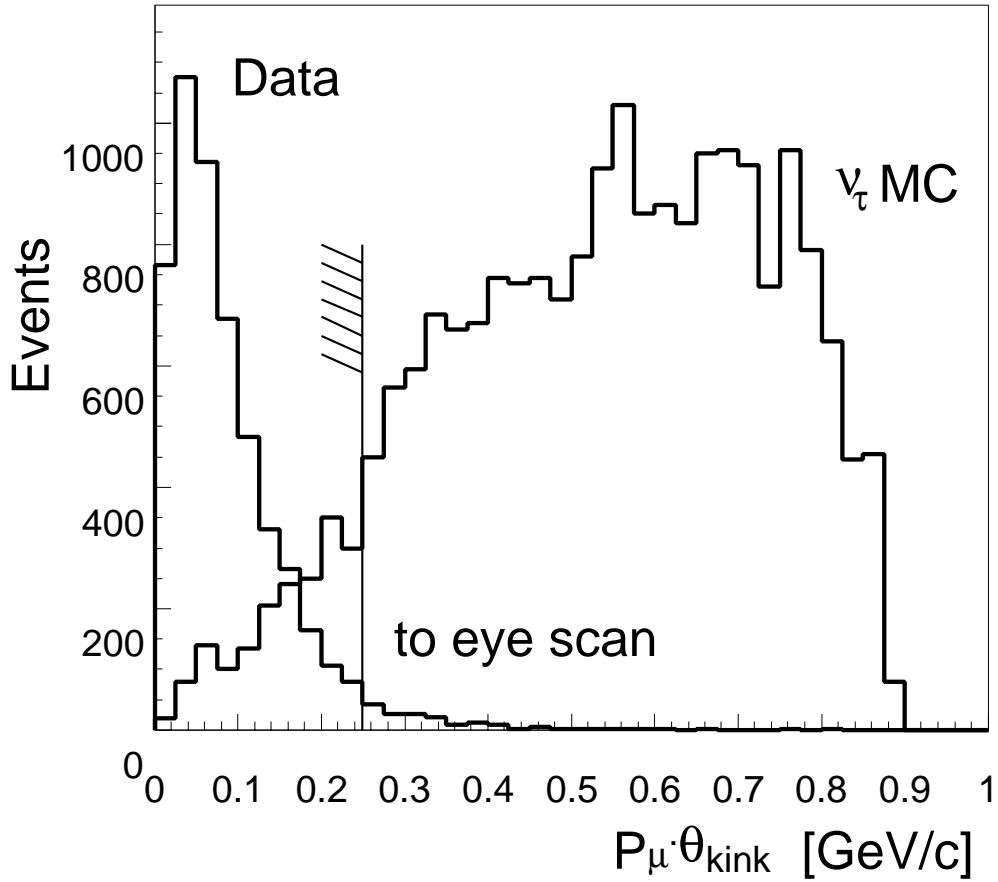


Figure 9: Distribution of  $p_\mu \cdot \theta_{kink}$  from simulated  $\nu_\tau$  interactions and real data. With a cut of  $p_\mu \cdot \theta_{kink} > 250$  MeV, most of the  $\nu_\tau$  interactions survive.

One of the main backgrounds for the single negative hadron mode is the scattering with no visible recoil of a negative secondary hadron produced in an NC interaction. This rate was estimated to be  $< 3 \times 10^{-6}$ . One-prong single hadronic decay of charmed particles in  $\bar{\nu}_e$  or  $\bar{\nu}_\mu$  interactions contribute to the background if the primary lepton is not identified. The rate of one-prong decay of charmed particles is  $< 0.5 \times 10^{-6} \times N^{CC}$ .

Therefore, the background contributions are negligible at the present level of statistics.

## 5 Present Status of the Analysis

The first run started in April 1994 and finished in October 1995. The second run with new emulsion started in April 1996 and finished in November 1997. From the measured characteristics of the beam, the statistics recorded up to now correspond approximately to 320,000 and 460,000  $\nu_\mu$  interactions in runs I and II, respectively.

So far, 120,000 charged current events have been analyzed, which corresponds to 10% of the full statistics. 14,897 events with a muon in the final state have been found in the emulsion and analyzed. For the single hadron channel, a first sample of 1,336 (4% of the full expected statistics) has been analyzed. No  $\nu_\tau$  interaction candidate was found.

## 6 Present Result

The oscillation probability is expressed as a ratio of observed  $N_\tau$  to  $N_\mu$  events, weighted by the ratio of both cross sections and corrected for acceptance, efficiency, and branching ratio for each decay channel. In the case of no observed  $\tau^-$  decay, the upper limit of the ratio is expressed as  $2.3/N_\mu$ . The value of 2.3 is obtained using Poisson statistics for observing no signal (90% C.L.).

The oscillation probability for large  $\Delta m^2$  is  $P(\nu_\mu \rightarrow \nu_\tau) = 1/2 \sin^2(2\theta_{\mu\tau})$ . The mixing angle is then expressed as:

$$\sin^2(2\theta) \leq 2 \cdot \frac{2.3}{N_\mu} \cdot \frac{\langle \sigma_\mu \rangle}{\langle \sigma_\tau \rangle} \cdot \frac{1}{\sum_{i=\mu^-, h^-} \frac{\langle A_i(\nu_\tau) \rangle}{\langle A(\nu_\mu) \rangle} \cdot \text{BR}_i \cdot \varepsilon_i \cdot r_i}$$

with  $A_i$  product of detector acceptance and efficiency,

$N_\mu$  number of scanned  $\nu \rightarrow \mu^-$  events with vertex found in the emulsion,

$\varepsilon_i$  kink-finding efficiency,

$r_i$  fraction of events of this class with respect to the  $\mu$ -channel.

The flux-weighted ratio of the average of the cross sections  $\langle \sigma_\mu \rangle / \langle \sigma_\tau \rangle$  is 1.89. The present values of the ratio of the acceptances, branching ratios, and kink-finding efficiencies depend on the decay channel and are shown in Table 1. The acceptances and efficiencies are Monte Carlo estimates.

| decay mode  | $\langle A_i \rangle / \langle A \rangle$ | BR <sub><i>i</i></sub> | $\varepsilon_i$ | $r_i$ |
|---|---|------------------------|-----------------|-------|
| $\tau^- \rightarrow \mu^- \bar{\nu}_\mu \nu_\tau$ | 1.07                                      | 0.17                   | 0.55            | 1     |
| $\tau^- \rightarrow h^-(nh^0)\nu_\tau$            | 0.36                                      | 0.50                   | 0.26            | 0.44  |

Table 1: Data used for the calculation of the oscillation limit.

With 14,897 events from the muon channel and 1,343 events from the single negative hadron channel, an upper limit of  $\sin^2(2\theta) \leq 4.5 \times 10^{-3}$  for large  $\Delta m^2$  is set.

## 7 Outlook

After four years of data taking, about 840,000  $\nu$ -CC events were recorded. For the muon channel, an improvement in sensitivity by a factor of ten is expected due to the statistics. With the present efficiency the  $0\mu$  channel gives an improvement by a factor of 1.5 alone. For the efficiency, like vertex location and kink finding, an improvement of 1.7 can be expected. In total, an improvement of approximately a factor of 25 with respect to the current muon channel result can be reached. The gain in statistics translates linearly into an improvement of sensitivity, since the background contribution is negligible. Therefore, the sensitivity for large  $\Delta m^2$  will eventually be  $\sin^2(2\theta_{\mu\tau}) \leq 2 \cdot 10^{-4}$ , which is a factor of  $\sim 20$  better than the present limit of E531 of Ushida *et al.*<sup>13</sup> The  $\Delta m_{\mu\tau}^2$  versus  $\sin^2(2\theta_{\mu\tau})$  parameter space explored by CHORUS, together with regions excluded by previous experiments,<sup>12</sup> is shown in Fig. 10.

## 8 Conclusion

Since April 1994 the CHORUS detector has successfully been taking data in the CERN Wide-Band Neutrino Beam. At present, 14,897 events with a negative muon in the final state and 1,336 events with a negative hadron in the final state have been analyzed. Since no oscillation signal was observed, an upper limit of  $\sin^2(2\theta) \leq 4.5 \cdot 10^{-3}$  at large  $\Delta m^2$  is given. Eventually, CHORUS will be capable of reaching an upper limit for the  $\nu_\mu \rightarrow \nu_\tau$  oscillation mixing angle of  $\sin^2(2\theta) \leq 2 \cdot 10^{-4}$  at large  $\Delta m^2$ .

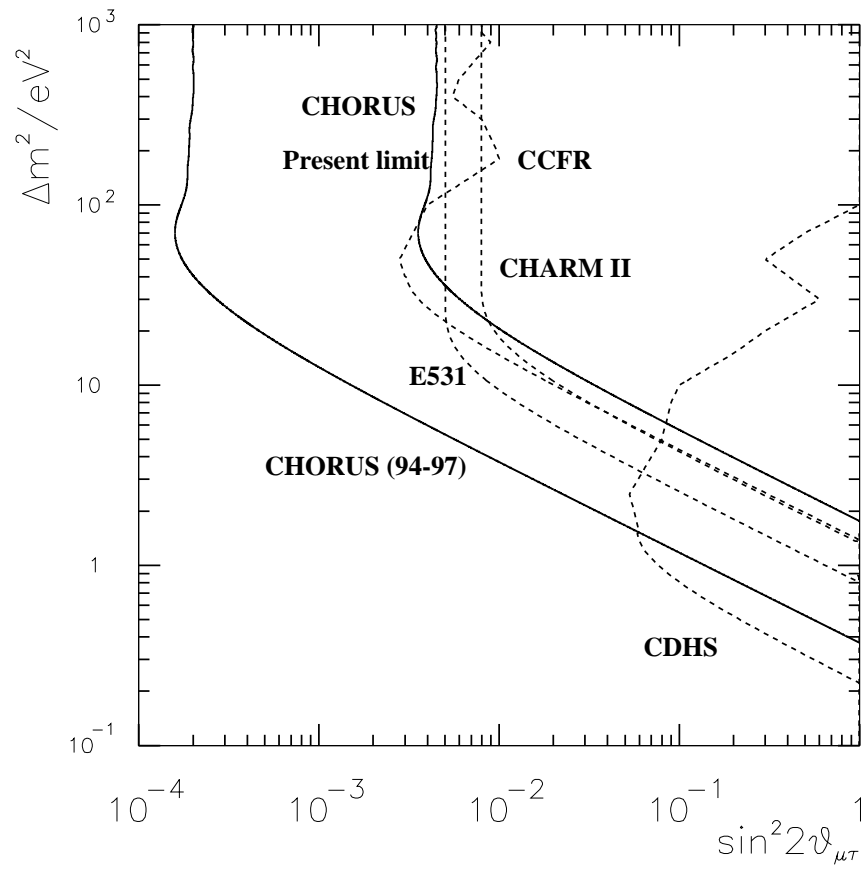


Figure 10: Exclusion plot for the  $\Delta m^2 - \sin^2(2\theta_{\mu\tau})$  parameter space.

## References

- [1] For an overview on this subject of neutrino physics, see, for example, *Neutrino Physics*, edited by K. Winter (Cambridge University Press, 1991);  
For the current status of neutrino physics, see, for example, *Proceedings of the XVII Int. Conf. on Neutrino Physics and Astrophysics, Helsinki 1996*, edited by M. Roos (World Scientific, 1996).
- [2] Ya. B. Zel'dovich and I. D. Novikov, *Relativistic Astrophysics* (Nauka, Moscow, 1967);  
H. Harari, Phys. Lett. B **216**, 413 (1989);  
J. Ellis, J. L. Lopez, and D. V. Nanopoulos, Phys. Lett. B **292**, 189 (1992);  
H. Fritzsch and D. Holtmannspötter, Phys. Lett. B **338**, 290 (1994).
- [3] B. Pontecorvo, Sov. Phys. JETP **6**, 429 (1958).
- [4] Z. Maki *et al.*, Progr. Theor. Phys. **28**, 870 (1962).
- [5] N. Armenise *et al.*, CHORUS Proposal, CERN-SPSC/90-42 (1990);  
M. de Jong *et al.*, CERN-PPE 93-131 (1993);  
E. Eskut *et al.*, Nucl. Instrum. Methods A **401**, 7 (1997).
- [6] NOMAD Proposal, CERN-SPSC/91-21 (1991), SPSC P261 (1991).
- [7] G. Acquistapace *et al.*, CERN-ECP/95-14 (1995).
- [8] B. Van de Vyver, Nucl. Instrum. Methods A **385**, 91 (1997).
- [9] P. Annis *et al.*, Nucl. Instrum. Methods A **367**, 367 (1995).
- [10] P. Annis *et al.*, Nucl. Instrum. Methods (to be published), CERN-PPE/97-100.
- [11] S. Buontempo *et al.*, Nucl. Instrum. Methods A **349**, 70 (1994).
- [12] N. Ushida *et al.*, Phys. Rev. Lett. **57**, 2897 (1986);  
M. Gruwe *et al.*, Phys. Lett. B **309**, 463 (1993);  
K. S. McFarland *et al.*, Phys. Rev. Lett. **75**, 3993 (1995);  
P. F. Loverre, Phys. Lett. B **370**, 156 (1996).
- [13] N. Ushida *et al.*, Phys. Lett. B **206**, 375 (1988).